Electrical Measurements in Molecular Electronics

Dustin K. James* and James M. Tour*

Department of Chemistry and Center for Nanoscale Science and Technology, MS 222, Rice University, 6100 Main Street, Houston, Texas 77005

Received March 2, 2004. Revised Manuscript Received June 18, 2004

This paper reviews the various methods used to measure the electrical characteristics of individual or small groups of molecules, including crossed-wire junctions, mechanically controllable break junctions, conducting atomic force microscopy, scanning tunneling microscopy, molecular electronics on silicon surfaces, the NanoCell, nanopores, and other devices. It is shown that in the most common embodiment, the metal−molecule−metal junction, the assembly must be considered in whole. The characteristics of the molecule cannot be easily separated from the metal electrodes connected to it or from the method used to do the testing. $I(V,T)$ data is necessary to rule out non-molecular transport mechanisms such as metal filament formation.

I. Introduction

Our group has been synthesizing compounds as molecular electronics candidates for over 15 years.[1] We have extensively reviewed our own work in molecular electronics[2] including the commercial aspects, chemistry, devices, and architectures.[3] Recent synthetic work has focused on the many possible perturbations of the oligo(phenylene ethynylene) (OPE) class of molecules. This work has included the combinatorial synthesis of OPEs,[4] the synthesis of nitrile-terminated OPEs,[5] biphenyl- and fluorenyl-based OPEs,[6] and orthogonally functionalized OPEs including azobenzenes and bipyridines, as well as members of the oligo(phenylene vinylene) (OPV) class of molecules.[7] Oligoanilines,[8] aryldiazoniums,[9] and ladder oligomers[10] have also been prepared for testing as molecular electronics candidates.

During this time it has become clear that even though the syntheses of multitudes of molecules have been laborious, the testing of the molecules in electrical devices has fallen far behind the pace of synthetic efforts. The design of new molecules is based on structure−activity relationships; therefore, the synthetic chemist needs testbed data that can be put into a synthesis feedback loop in order to prepare new candidates based on what is thought to be the mechanism(s) of action in the devices. Many different testbeds, some of which we will review here, have been developed. The combination of different testbeds and different classes of molecular electronic candidates has led to numerous publications in the field with results and measurements that are difficult to filter in order to draw logical conclusions.

Metzger,[11] Gorman,[12] Weiss,[13] and Salomen et al.[14] recently published excellent reviews on the field of molecular electronics. In this review, we will focus on testing that has been done on alkanethiols and conjugated aromatic molecules such as OPEs or OPVs since 2000. The majority of the research has been done on self-assembled monolayers (SAMs) of these molecules. The testbeds used include crossed-wire junctions, mechanically controllable break junctions, conducting atomic force microscopy (cAFM), scanning tunneling microscopy (STM), molecular electronics on silicon surfaces, the NanoCell, nanopores, and other devices.

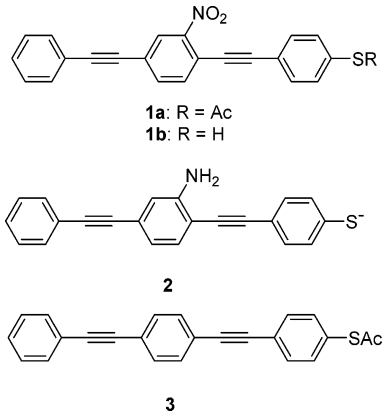

Figure 1. SAMs formed from **1a** under basic conditions were found to contain ∼30% of **2**. SAMs formed from **1a** or **3** under acidic conditions or from **1b** under neutral conditions were not contaminated by **2**.

II. SAM Formation−A Caveat

The chemistry of SAM formation has been carefully studied,[15] and it has been found that the use of basic conditions to deprotect the thioacetyl-protected molecule **1a**, Figure 1, led to mixed SAMs containing ∼30% of the OPE **2** apparently from oxidation of the S atoms coupled to reduction of the nitro moiety. Assembly of the pure SAM from the thioacetate **1a** under acidic conditions or from the thiol **1b** in solvent without acid produced well-ordered SAMs with an average molecular tilt of 32−39° from the surface normal. The unsubstituted OPE **3** also formed well-ordered SAMs with a tilt of ∼33°. The SAMs formed from **1a** or **1b** showed significant chemical instability under storage in air and/

* Authors to whom correspondence should be addressed. E-mail: dustin@rice.edu (D.K.J.); tour@rice.edu (J.M.T.).

10.1021/cm049648r CCC: $27.50 © 2004 American Chemical Society
Published on Web 08/31/2004

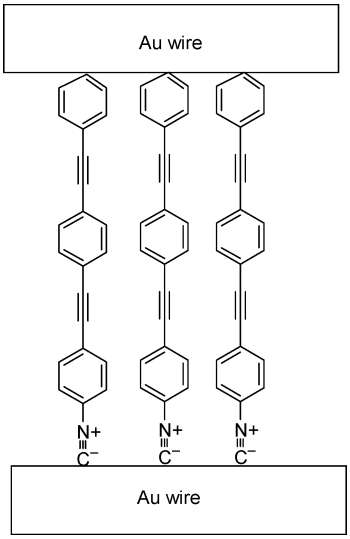

Figure 2. Metal−molecule−metal junction in the crossed-wire apparatus for measuring conductance of SAMs on Au wires.

or with light exposure. It was concluded that extreme care must be used when devices are made with these or similar molecules to ensure that they are handled under the appropriate conditions and that SAMs from assembly of nitro-based molecules by deprotection of thioacetyl groups under basic conditions must be carefully analyzed for impurities. It is preferable to use acid conditions for the deprotection of nitro-containing OPEs.[16]

III. Crossed-Wire Junction Measurements

Kushmerick and co-workers measured the conductance of conjugated molecules in a SAM between two Au crossed wires at room temperature.[17] To form the test junction shown in Figure 2, a SAM of isonitrile OPE molecules was formed on one 10-μm diameter Au wire and a second 10-μm diameter Au wire was brought into contact with it by passing DC current through the first wire in the presence of a magnetic field, causing it to be deflected. When the two wires touched, the *I(V)* characteristics of the metal−molecule−metal junction could be determined. As the deflection current increased, the *I(V)* characteristics of the junction changed, with increasing current at higher deflection of the wire. At low deflection loads the number of molecules calculated to be in the junction was in good agreement with the power law scaling expected from Hertzian contact mechanics. The data at higher loads was not consistent with this simple model, indicating that the mechanism of charge transport might be changing from through-bond to through-space charge transport or that the molecules in the SAM were being structurally deformed at high loads, resulting in a modification of their highest occupied molecular orbital (HOMO)−lowest unoccupied molecular orbital (LUMO) gap. A third cause of the change at high load might be the formation of multiple contacts between the Au wires. By dividing the current at each deflection load by the number of molecules calculated to be in the junction at that load, the conductance curves collapsed into a common single curve, indicating that there was a linear dependence of conductance on the number of molecules in the junction. No *I(V,T)*[18] work was done to verify the conductance

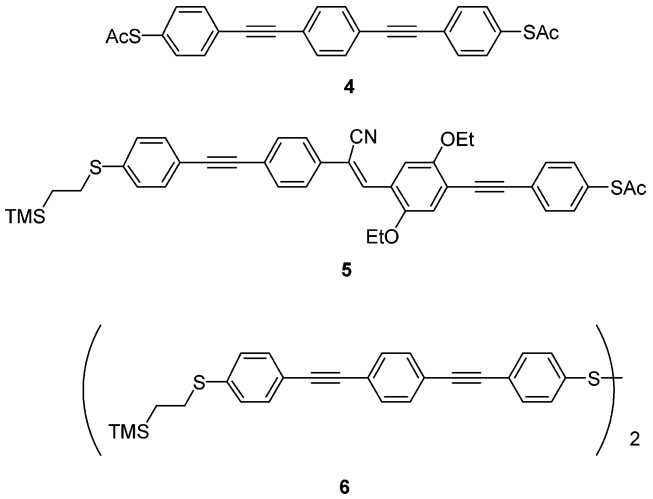

Figure 3. Molecules studied in the crossed-wire junction testbed.

mode in this crossed-wire testbed work. Without the temperature-dependent data, transport mechanisms cannot be determined.

In Kushmerick's work, negative differential resistance (NDR) was not observed. NDR is a separate effect from conductance switching.[19] In electrical circuits, the ratio of the voltage across a circuit to the current through it is the static resistance; this ratio can change with variation in either voltage or current. The ratio of the voltage differential to the current differential is the dynamic resistance of the circuit. When over certain voltage ranges the current decreases as the voltage increases, that range of voltages is known as the negative differential region. NDR has been observed in metal−molecule−metal junctions.[3] In conductance switching the circuit is either ON or OFF, with no negative differential regions observed.

The crossed-wire junction technique was also used to measure the charge transport of the OPEs **3** and **4** (Figure 3).[20] The metal−molecule−metal junction formed from **4** would be symmetric, while the junction formed from **3** is not. The measured conductances show that the symmetric molecule **4** acts as a molecular wire, with transport characteristics the same in both directions, while the asymmetric molecule **3** had the characteristics of a molecule-based diode, due to the connections at either end being dissimilar. Since the metal contacts were both Au, it was the metal−molecule connection itself that affected the transport properties of the assembled junction.

The two molecules **5** and **6** (Figure 3) were used in sequential deprotection deposition processes[21] in the crossed-wire junction so that the dipole of the asymmetric molecule could be oriented in a deliberate manner. Previous work has shown that disulfides such as **6** form SAMs that are equivalent to those derived from their parent thiols,[22] although it is possible that there may be differences in the solubility of the disulfide compounds, as we have seen with polymerization of OPE dithiols under trace oxidizing conditions.[23] To establish that deliberate orientation and sequential deprotection was taking place, a SAM of **6** was formed on a Au-coated quartz crystal microgravimety (QCM) oscillator crystal by immersing the QCM crystal in a solution of **6** in THF for 24 h. The SAM, with the second

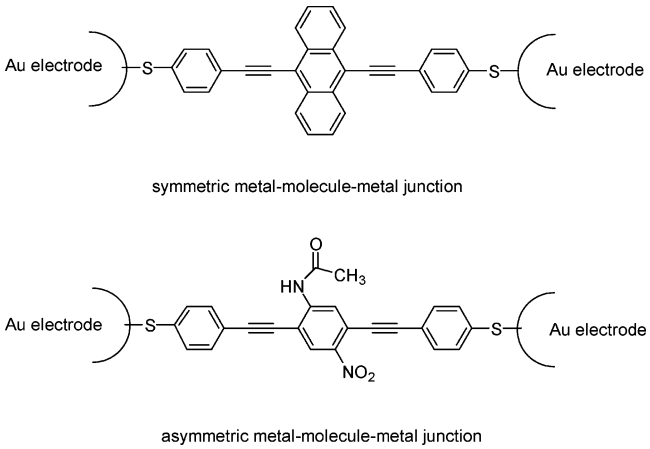

Figure 4. Symmetric anthracene-based metal−molecule−metal junction (top) and the asymmetric nitro acetylamine metal−molecule−metal junction (bottom) studied in a mechanically controllable break junction.

thiol group still protected by the ethyl−TMS group, was exposed to 6 nm Au nanoparticles, leading to an increase in surface mass of 0.71 ng cm^{-1}. The Au nanoparticles were easily washed off by a water rinse of the oscillator crystal, indicating that they were only physisorbed. Deprotection of the second "top" thiol group by fluoride followed by exposure of the SAM on the QCM crystal to the nanoparticles a second time resulted in 1.06 ng cm^{-1} increased mass that was not removed by water rinses, clearly showing that the nanoparticles had become part of a strong metal−molecule−metal junction. Hence, the orthogonal thiol deprotection scheme developed by Pollack et al. is quite effective.[21]

A SAM of **5** in the crossed-wire junction testbed displayed asymmetric bias polarity when the *I(V)* characteristics were tested, indicating slight rectification of the tunneling current. The metal−molecule−metal junction prepared from **6** displayed no rectification.

IV. Mechanically Controllable Break Junction Measurements

Since our work measuring the conductance of a single molecule of benzene-1,4-dithiol in a mechanically controllable break junction,[24] more complex metal−molecule−metal junctions, shown in Figure 4, have been tested by Reichert et al. at room temperature[25] and at low temperature,[26] and a quantum mechanical model has been developed to correlate the data.[27] For the symmetric metal−molecule−metal junction shown in Figure 4, the *I(V)* data would be expected to be symmetric with respect to voltage inversion. For the asymmetric metal−molecule−metal junction, however, the current in the positive or negative direction should produce an asymmetric voltage response along the molecule. The experimental data supported this hypothesis; careful manipulation was required, but the symmetric molecule produced symmetric *I(V)* curves while the asymmetric molecule did not. Sample-to-sample fluctuation was observed at room temperature, leading the authors to conclude that consideration of the characteristics of the entire metal−molecule−metal junction was important to the successful duplication of measurements. The low-temperature (∼30 K) conductance measurements were much more stable, and the data had narrower line widths and less noise. At both temperature ranges the authors conclude that current through single molecules was measured, although *I(V,T)* measurements were not taken throughout a temperature range as required to accurately determine the transport mode.[18] NDR was not observed.

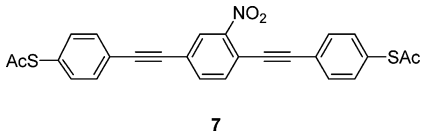

7

Figure 5. Nitro-functionalized OPE **7** used in cAFM studies by Rawlett.[31]

V. Conducting Atomic Force Microscopy (cAFM)

Frisbie and co-workers used conducting atomic force microscopy (cAFM) to probe SAMs of alkanethiols on Au,[28] alkane- or benzylthiols on Au,[29] and alkane- or oligophenylene (OP) thiols on Au.[30] In cAFM, an AFM tip, coated with metal, is put in direct contact with the material to be probed using a controlled load force. The probe is positioned using normal force feedback, thus disconnecting the sample conductivity from the probe positioning methodology. Using cAFM the metal−molecule−metal junctions were found to behave as tunneling junctions, with the resistance to current increasing exponentially with SAM thickness. Resistances were 10 times lower for junctions based on benzylthiol SAMs compared to hexanethiol SAMs of the same thickness.

For the OP and alkanethiol SAMs formed on Au surfaces, the electronic decay constant values or tunneling decay parameter[14] (β), using Au probe tips at constant applied load, were determined. The β value is a measure of how much current is lost per unit length of each molecule. The β value for the OP SAMs was 0.42 $\pm$ 0.07 $Å^{-1}$, while that for the alkanethiolate SAMs was 0.94 $\pm$ 0.06 $Å^{-1}$. For alkanethiol bilayer junctions (wherein the AFM tip was coated with a SAM of alkanethiols in addition to the metal surface) the β value was 1.07 $Å^{-1}$. The β values indicated that electronic transport through conjugated systems was easier than through nonconjugated systems.

Rawlett and co-workers[31] inserted functionalized OPE and nonfunctionalized OPE dithiol molecules **7** (Figure 5) and **4**, respectively, into defect sites of dodecanethiol SAMs and then assembled Au nanoparticles on the unreacted top thiol and used cAFM to measure the conductance of the individual molecules. The experiments were run at room temperature in air. The unfunctionalized **4** showed no NDR characteristics, while the nitro-functionalized **7** displayed reproducible NDR at two different labs. The scans degraded over time, presumably due to oxidation of the molecules in the air under the high voltages used.

Using cAFM Lindsay and co-workers[32] found that the probe tip and the force with which it contacts the molecular film on the surface of the metal are important factors in the measured electrical characteristics of the film. The current through alkanethiol films depended on the cAFM tip contact force, see Table 1, and was accounted for by film deformation, with the compression of the film increasing the chain-to-chain electron tun-

Table 1. Variation of Decay Constant with cAFM Tip Contact Force[32]

entry	contact force, nN	decay constant, β_n
1	4.5	0.8
2	6	1.0
3	8	1.1
4	14	1.2

neling. Chain-to-chain tunneling, in which electrons pass from one alkanethiol molecule to its neighboring molecule, was differentiated from through-bond electron tunneling, which occurs through the backbone of individual molecules. The electronic decay constant β for current passing through a barrier in through-bond tunneling is about 0.9 $Å^{-1}$ (1.14 per methylene unit for alkanethiols), while for chain-to-chain tunneling it is about 1.3 $Å^{-1}$.[33] Lindsay's data indicated that long-chain alkanethiol films were not as sensitive to higher tip contact force as the short chains. Conversely, 1,8-octanedithiol films were not at all sensitive to contact force, perhaps because the top thiol alligator clip formed a Au−S bond with the cAFM tip. Thus, the method by which current is measured as well as the nature of the molecule in the SAMs can greatly affect the measured properties.

The research of Tao and co-workers[34] supports the conclusion that the entire metal−molecule−metal assembly is important to consider in interpreting electrical measurements. A Au-coated Si cAFM tip was moved into and out of contact with a Au surface in a toluene solution of either 1,8-octanedithiol or 4,4′-bipyridine. The conductance of the metal−molecule−metal junction could be measured as well as the force applied to the molecule. As the moving cAFM tip was pulled away from the junction, the conductance decreased in discrete steps. The stepped decrease in conductance was interpreted as the molecule pulling away from the Au cAFM tip and bringing a Au atom with it, such that a string of Au atoms was formed between the molecule and the Au surface until the connection was broken. As each Au atom was pulled out of the Au surface, the conductance dropped. The force being applied to the molecule as it was pulled out of the Au surface decreased in sawtooth-shaped waves with the maximum pulling force corresponding to the point just before the conductance dropped. This correspondence of force with conductance was logical since one would expect that the force necessary to remove a Au atom from the Au surface would be at its greatest just before it was pulled away; just after being pulled away, the conductance through the metal−molecule−metal junction should drop. Note that this procedure is different than the prior methods discussed since the molecules in question had alligator clips on both ends, with the top alligator clip bonding to the Au surface on the cAFM tip.

VI. Scanning Tunneling Microscopy

Many researchers have used scanning tunneling microscopy (STM) to probe the electrical response of molecular electronics candidates; the field has been recently reviewed.[35] In 1999 we reported on the placement of OPEs in an alkanethiol matrix by STM lithography,[36] using STM tip voltage pulses to remove molecules from an alkanethiol SAM on Au in the presence

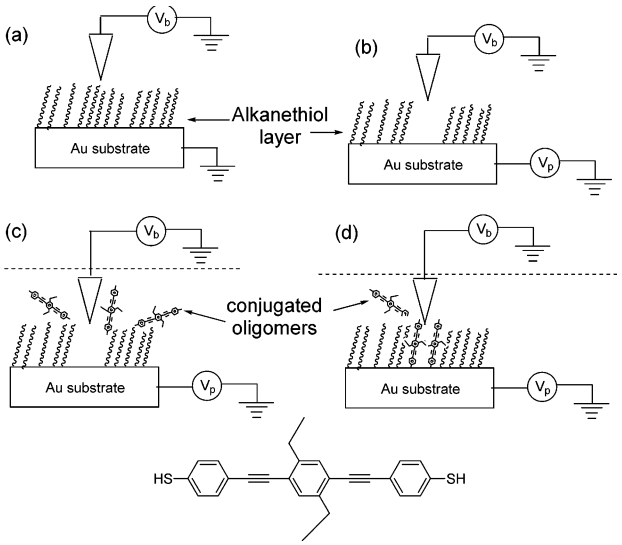

Figure 6. (a) Alkanethiol SAM is formed on Au; (b) STM tip is used to form patterns in the SAM by selectively removing molecules from the SAM. (c) The same process is done under a solution containing OPEs that are inserted in the formed patterns in d.

of dissolved OPEs, which were deposited from solution onto the sites cleared by the STM tip, see Figure 6.

It was subsequently found that mixed alkanethiol/OPE SAMs could be formed on Au by exposing alkanethiol SAMs to a solution of the OPEs ∼15−40 Å in length without the need for STM lithography.[37] The OPEs were individually inserted into boundaries between SAM structural domains and in bundles at substrate step edges, see Figure 7. The SAMs were characterized by STM and high-sensitivity infrared reflection spectroscopy. It was found that the alkanethiolate ordering of the host SAM was retained after insertion. The inserted OPEs of lengths ∼15 Å adopted surface orientations similar to those of the alkanethiolates at all concentrations, including pure OPE SAMs. An OPE that was ∼40 Å long had a tilt angle to surface normal of about 55° in its pure SAM; the tilt angle approached that for a SAM of pure octanethiol (30°) as the concentration of the ∼40 Å molecule was decreased. The data indicated that the alkanethiolate SAMs were densely packed around the short ∼15 Å OPEs. For mixed SAMs that were not tightly packed, vapor-phase annealing could be used to reinsert alkanethiolate molecules around OPEs that have been placed at defect sites and step edges.[38]

Using STM to track over time the conductance switching of single and bundled OPEs[39] **1a**, **3**, and **8** (see Figure 8) isolated in matrixes of alkanethiolate SAMs, we found that the ON or OFF state persisted for periods of seconds to tens of hours. When the surrounding matrix was well ordered and tightly packed, the molecules switched less often than when the surrounding matrix was poorly ordered. The data led to the conclusion that the switching phenomenon was due to conformational changes in the molecules or bundles rather than electrostatic effects of charge transfer. The more tightly packed molecules or bundles did not have as much room to change conformations, while the poorly packed molecules or bundles had more room and thus were able to switch ON and OFF more frequently.

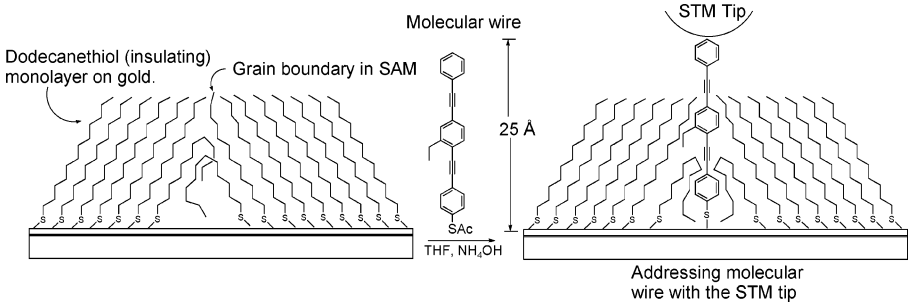

Figure 7. Insertion of OPEs into grain boundaries of SAMs.

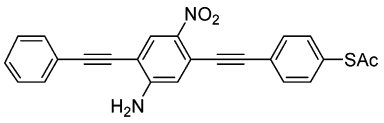

8

Figure 8. Conductance switching of **8**, along with **1a** and **3**, was followed by STM for SAMs of the molecules on Au. The ON or OFF state for isolated and bundled molecules persisted for periods of seconds to tens of hours.

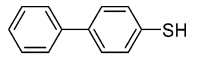

9

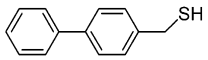

10

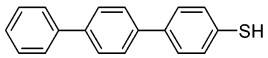

11

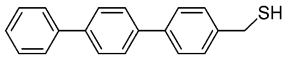

12

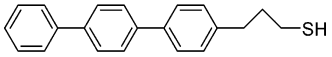

13

Figure 9. OP thiol derivatives studied by STM.

The electrical conduction of OP thiol derivatives with zero, one, or three methylene groups between the thiol and the aromatic ring were examined by STM.[40] The molecules shown in Figure 9 were inserted into defects in C9 alkanethiol SAMs. The height differences between the C9 alkanethiol domains and the domains created by the aromatic molecules depended on the size of the aromatic domain. The height difference became larger as the domain of aromatic molecules in the mixed SAM became larger. However, for domains of the same size, the mixed SAMs made from molecules without the methylene group between the thiol and the aromatic ring tended to be shorter than the SAMs containing molecules containing one methylene group. The molecules with one methylene group were thought to form a more ordered SAM with higher crystallinity, because the methylene group allowed the rest of the molecule to stand more upright and thus form a more uniform height, while the domains formed in the mixed SAMs by the molecules without methylene groups tended to be more disordered. The data indicated that vertical conduction in the SAM increased with one methylene group between the thiol and aromatic ring.

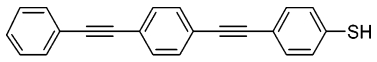

14

Figure 10. Analysis by STM found that OPE thiol **14** had a tilt angle of 5° from the surface normal in SAMs.

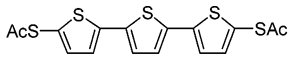

15

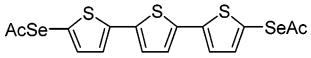

16

Figure 11. Molecules **15** and **16** used to study the electronic characteristics of the alligator clip S and Se by STM.

The lateral conductivity in large domains of mixed SAMs of **12** imbedded in C9 or C12 alkanethiols was estimated using STM and found to be larger than 0.01 S/cm.[41]

The OPE thiol **14**, Figure 10, has been shown to form very well ordered SAMs by STM.[42] Comparison of the height of the OPE thiol domains in mixed SAMs to alkanthiol domains with known heights allowed the tilt angle of the molecules to be estimated. Contrary to the tilt angle of 30° from the surface normal for alkanethiols (and to our work for the same compound[15]), the OPE thiol was reported to have a tilt angle of 5° from the surface normal.

Alkanethiol SAMs formed of molecules with the electroactive headgroups ferrocene and galvinol displayed NDR when the *I(V)* response was measured using a STM tip−molecule−metal junction[43] under dodecane solvent. The NDR response was equivalent in single-component SAMs and in patterned monolayers.

Using STM experiments in air and ultrahigh vacuum (UHV), a Se alligator clip on terthiophene provided better molecule−metal electronic coupling than the standard S alligator clip.[44] This result differs from theoretical studies[45] where the S was found to be slightly better than a Se alligator clip. To perform this STM testing, bisthiolterthiophene **15** or bisselenolterthiophene **16**, shown as their protected precursors in Figure 11, was inserted into defect sites on a dodecanethiol SAM.

The azo-containing molecule shown in Figure 12 was inserted into defect sites of a dodecanethiol SAM.[46] The molecule is capable of isomerizing about the azo linkage from trans to cis and back again; when in the trans form the dipole is aligned in the direction of the long axis of the molecule, while in the cis form the dipole is tilted from the molecular axis. Because of the dipole, the

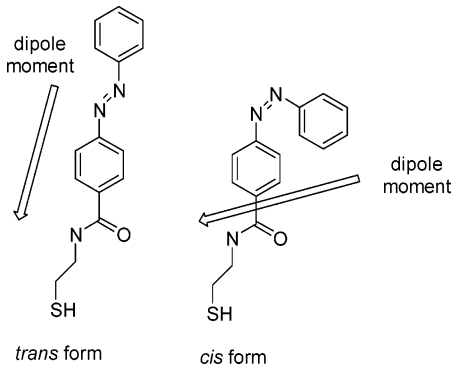

Figure 12. Azo-group containing molecule studied by STM. Isomerization of the azo linkage converts the trans form to the cis form and back.

electric field applied between the substrate and the STM tip is expected to influence the molecular conformation. A STM image of the azo molecules embedded in a dodecanethiol SAM at the sample bias voltage of +1.0 V show bright protrusions of the azo molecules. Another STM image was taken at a sample bias voltage of −1.0 V. Azo molecules which were surrounded by tightly packed dodecanethiol molecules exhibited negligible changes in brightness; however, those in less tightly packed areas such as etch pits or phase boundaries appeared darker in the image. This suggests that a conformation change took place. A *I(V)* measurement taken over an unchanged azo molecule was fairly symmetric, while that taken over a changed azo molecule shows a high-conductivity state and a low-conductivity state in the high-positive voltage region. The high-conductivity state was attributed to the trans isomer, while the low-conductivity state was attributed to the cis isomer. The inverse decay lengths obtained by *I(V)* measurement for the azo molecules was 8.5 ± 1.6 nm^{-1} for the high-conductivity state and 5.2 ± 1.3 nm^{-1} for the low-conductivity state.

The random switching seen in OPE molecules during STM experiments[39] has been attributed to changes in ring conformations molecular tilting or electron delocalization or a combination of the three. On the basis of their work with analysis of alkanedithiols inserted into alkanethiol SAMs on Au surfaces whose top thiol group was addressed by deposition of Au nanoparticles followed by probing with a Pt−Ir STM tip, Lindsay and co-workers proposed a bond-fluctuation mechanism whereby the switching is caused by the "blinking" (bond breakage and formation) of a thiol−Au bond. The molecules tested are shown in Figure 13.

Comparison of the switching rates of the alkanedithiols and the OPE dithiol with and without the top nanoparticle contact confirmed that some switching events were associated with fluctuations of the top contact but others were intrinsic to the molecule as inserted in the matrix and attached to the underlying Au. Prior work had shown that conductance of alkanedithols wired into a circuit with Au nanocontacts was not affected by relatively large stresses,[32] so the authors thought it was unlikely that an internal electronic process could turn off the tunneling conductance through the molecules. On the basis of all the data obtained, the authors concluded that the switching was caused by breaking and forming of the thiol−Au bond at the bottom contact of the dithiol molecule.

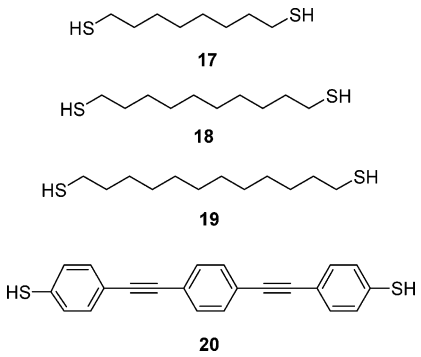

Figure 13. Molecules **17**−**20** tested by Lindsay and co-workers in developing their bond-fluctuation mechanism theory.

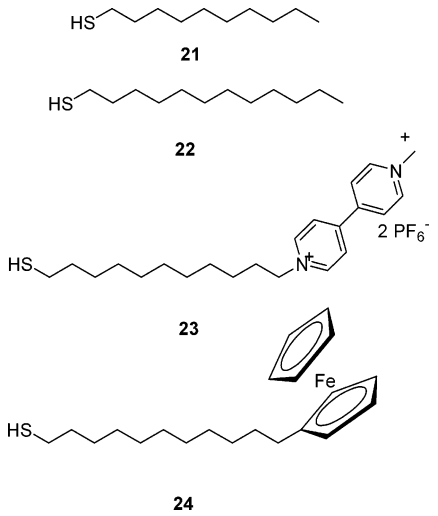

Figure 14. Molecules **21**−**24** that showed random switching in STM experiments by Gorman and co-workers.

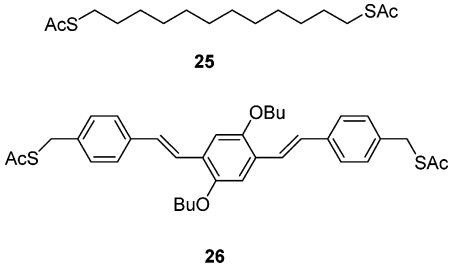

Figure 15. Protected alkanedithiol **25** and OPV dithiol **26** for which conductances were compared with that of **4** using STM.

Gorman and co-workers used STM to observe random switching events in the set of molecules shown in Figure 14.[47] The same researchers attenuated the NDR seen in such molecules by capping the electroactive ferrocene group with β-cyclodextrin or by functionalizing the STM tip used to probe the SAM with alkanethiols of varying lengths.[48]

Blum and co-workers compared the conductivity of **4** with **25** and **26**, shown in Figure 15, using STM and found that the order of conductance was OPV **26** > OPE **4** > C12 dithiol **25**.[49] The measured gap resistance was the same for OPE **4** in a crystalline SAM as it was for OPE **4** inserted into an undecanethiol matrix. The authors concluded that electron transport occurred through individual molecules and not by intermolecular

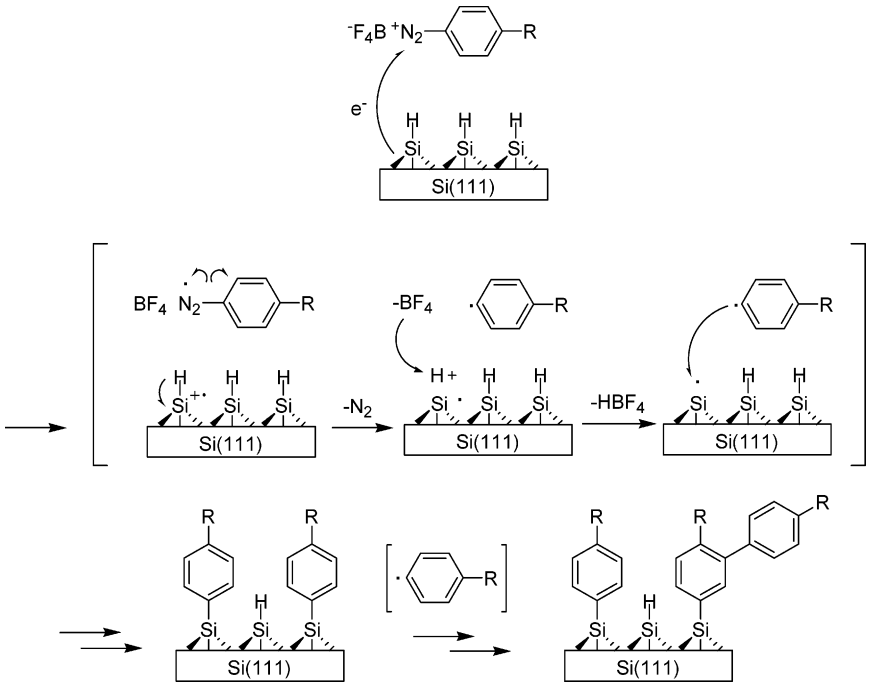

Figure 16. Example of spontaneous diazonium activation by a hydrogen-passivated Si(111) surface. An electron transfer from the surface at the open circuit potential generates a diazenyl radical and then an aryl radical upon loss of N_2. The complementary oxidative process generates a proton, which eliminates as HBF_4. The radical generation process results in side products such as reduced aromatics (by aryl radical attack of the Si−H surface) and the formation of covalently bound multilayers. FTIR evidence shows the loss of an average 65% of the surface hydride residues in the process of aryl radical generation. The multilayer formation can be retarded by the addition of BHT in situ, which may intercept the excess aryl radicals before they can attack the nascent monolayer.

hopping; however, no *I(V,T)* measurements were discussed.

VII. Molecular Electronics on Silicon Surfaces

Although a great amount of synthetic effort is spent on the design of electronically active organic molecules, often the overall performance of molecular devices is dominated by poorly formed contacts.[3] This has created more interest in ways of directly interfacing molecules with materials using high-quality contacts. Using aryldiazonium salts that are air stable and easily synthesized,[50] a room-temperature route to direct covalent bonds between π-conjugated organic molecules on oxide-free silicon hydride surfaces (Si−H_x) has been demonstrated.[51] The Si can be in the form of single-crystal Si including heavily doped p-type Si, intrinsic Si, heavily doped n-type Si, on Si(111) and Si(100), and on n-type polycrystalline Si. A data-encompassing explanation for the mechanism suggests diazonium activation by reduction at the open-circuit potential with aryl radical secondary products bonding to the surface, Figure 16.

The formation of the aryl−silicon bond attachments was confirmed by corroborating evidence from ellipsometry, reflectance FTIR, XPS (Figure 17), cyclic voltammetry (Figure 18), and AFM analyses of the surface-grafted monolayers. This spontaneous diazonium activation reaction offers an attractive route to highly passivating, robust monolayers and multilayers on many surfaces that allow for strong bonds between carbon and surface atoms with molecular species that are near perpendicular to the surface.

Aryldiazonium tetrafluoroborates such as molecule **27** were used to analyze the assembly characteristics and

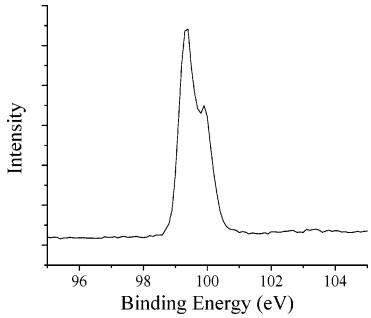

Figure 17. XPS spectrum of Si 2p region of n^{2+}-type Si(111) reacted with **27**, taken at a 30° takeoff angle, has a clear $2p^{1/2}$−$2p^{3/2}$ doublet and is free of the oxidation signal normally seen at around 103 eV.

resultant surface analytical properties of the zero-potential grafting reaction. Studies of the mechanism

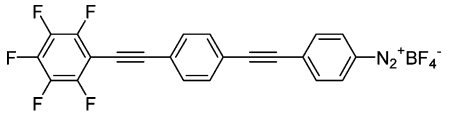

27

of the reaction reveal that it is mediated by the production of free-radical fragments from the diazonium salt precursor that bond to the surface of Si−H. The layer, according to surface analyses, is free of oxide contamination and possesses a low density of pinhole defects. Covalently bound organic monolayers on oxide-free Si offer possibilities for new applications in processing, electronic transport, and antistiction coatings for polysilicon-based microelectromechanical systems (MEMS) and nanoelectromechanical systems (NEMS) devices. They may also serve as a platform to study through-

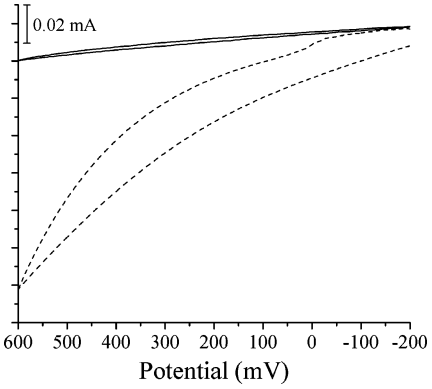

Figure 18. CV scans of reacted samples using 0.01 M $Fe(CN)_6^{3/4-}$ redox couple in 0.1 M $KClO_3$, with 1 cm^2 area exposed. In the above traces, an n^{2+}-type Si(111) wafer reacted with **27** (solid line) shows decreased ion current compared to Si(111):H surface (dashed line). The reference was a saturated calomel electrode.

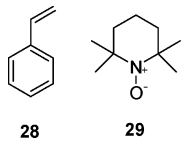

28 **29**

Figure 19. Styrene **28** and TEMPO **29** showed NDR characteristics when placed on degeneratively doped Si(100) surfaces.

bond interactions between molecules chemisorbed on surfaces and the bulk materials to which they are attached. Current work includes improving the long-range order of the surface assemblies, determining molecular effects on the electronic structure of the interfaces, and adapting molecular assemblies with reported NDR properties into silicon-based hybrid molecular electronic devices[52,53] to assess molecular vs interfacial-based device behavior.

Using UHV STM, Hersam and co-workers observed room-temperature NDR through individual molecules on degeneratively doped Si(100) surfaces.[54] For styrene molecules on n-type Si(100), NDR was observed only at negative sample bias; positive sample bias led to desorption of the molecules. Desorption did not occur at either positive or negative sample bias when the saturated molecule 2,2,6,6-tetramethyl-1-piperdinyloxy (TEMPO) was used, see Figure 19. NDR was observed only at negative sample bias for TEMPO on n-type Si(100) and only at positive sample bias on p-type Si(100). The authors concluded that the unique behavior was consistent with a resonant tunneling mechanism via molecular orbitals; however, no *I(V,T)*[18] studies were done.

VIII. NanoCell

Most proposed architectures based on molecular electronics are dependent upon precise order and building devices with exact arrays of nanostructures (i.e., molecule-embedded crossbars) painstakingly interfaced with microstructure.[3] Conversely, the NanoCell approach, as previously described[55] and simulated,[56] is not dependent on placing molecules or nanosized metallic components in precise orientations or locations. The internal portions are, for the most part, disordered, and there is no need to precisely locate any of the switching elements. The nanosized switches are added in abundance between the micrometer-sized input/output electrodes (Figure 20), and only a small percentage of them need to assemble in an orientation suitable for switching. NanoCells are disordered arrays of metallic islands that are interlinked with molecules between micrometer-sized metallic input/output leads. The assembled NanoCell exhibits reproducible switching behavior and two types of memory effects at room temperature (Figures 21−23). The switch-type memory is characteristic of a destructive read, while the conductivity-type memory features a nondestructive read. Both types of memory effects are stable for more than 1 week at room tem-

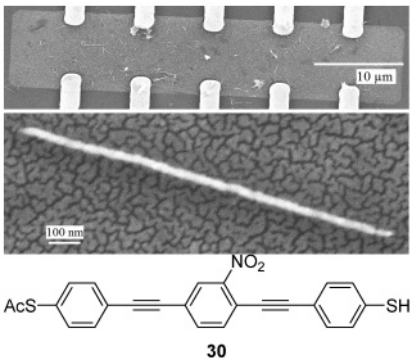

30

Figure 20. SEM image of the NanoCell after assembly of the Au nanowires and **30**. (top) Five juxtaposed pairs of fabricated leads across the NanoCell, and some Au nanowires are barely visible on the internal rectangle of the discontinuous Au film. (bottom) Higher magnification of the NanoCell's central portion showing the disordered discontinuous Au film with an attached Au nanowire.

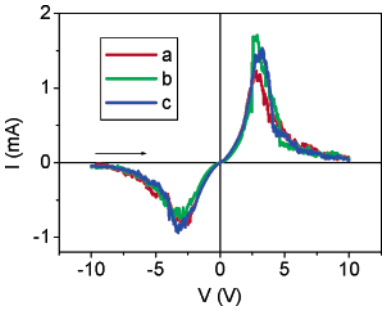

Figure 21. *I(V)* characteristics of the NanoCell at 297 K. The curves for a, b, and c are the first, second, and third sweeps, respectively (~40 s/scan). The PVRs in c are 23:1 and 32:1 for the negative and positive switching peaks, respectively. The black arrow indicates the sweep direction of negative to positive.

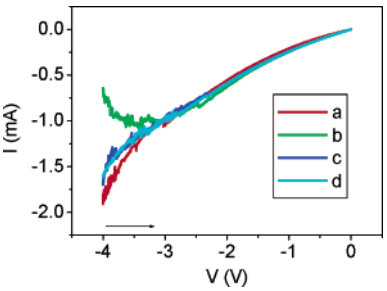

Figure 22. *I(V)* characteristics of the NanoCell before (a) and after (b−d) three voltage pulses at −8 V at 297 K. Curves b, c, and d were the first, second, and third scan (after the −8 V reset pulses), respectively. Scans a−d were run at ~40s/scan. The results here are from the same device used to generate the *I*(*V*) curve in Figure 21.

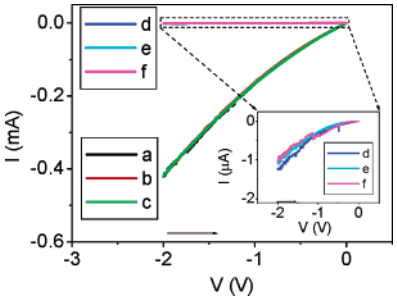

Figure 23. *I(V)* characteristics of the NanoCell before (scans a−c) and after (scans d−f) three voltage set pulses of −8 V at 297 K. The initial high σ state (0 state) is represented by curves a, b, and c, which are the first, second, and third scans before the set pulse, respectively. The low σ state (1 state) is represented by curves d, e, and f, which are the first, second, and third scans after the −8 V set pulses, respectively. The inset shows scans d−f in the μamp range. Scans a−c were run at ~40 s/scan. Scans d−f were run at ~50 s/scan. This is the same device as depicted in Figures 21 and 22.

perature, and bit level ratios (0:1) of the conductivity-type memory have been observed to be as high as 10^4:1 and reaching 10^6:1 upon ozone treatment that likely destroys extraneous leakage pathways. Both molecular electronic and nanofilamentary metal switching mechanisms have been considered, though the evidence points more strongly toward the latter. The NanoCell approach demonstrates the efficacy of a disordered nanoscale array for high-yielding switching and memory, while mitigating the arduous task of nanoscale patterning. *I(V,T)* measurements on a NanoCell indicated that the mode of electronic conductance was metallic or thermionic emission-based, depending on the set-state of the device.

IX. Nanopore

With our collaborator Reed we measured NDR in an OPE-based SAM contained in a nanopore[57] and demonstrated memory based on molecular random access memory.[58] The nanopore, shown in Figure 24, was constructed by etching, via e-beam, a small hole 30−50 nm in diameter in a silicon nitride membrane. The conditions of the etch were such that a bowl-shaped geometry was produced, with the hole at the bottom of the bowl. The bowl was then filled with evaporated Au, and the device was placed in a solution of the functionalized OPE. After allowing the SAM to form under basic conditions for 48 h, the device was removed from the solution, quickly rinsed, and placed on a liquid nitrogen cooling stage for the deposition of the bottom Au electrode via evaporation. The device was then diced into individual chips that were bonded onto packaging sockets. The electrical characteristics of the packaged testbeds were measured in a variable-temperature cryostat using a semiconductor parameter analyzer.

The *I(V)* characteristics of the Au−molecule−Au device for one molecule tested, shown in Figure 24, included a peak current density of ~50 A/cm^2; the NDR was ~−400 $\mu\Omega$ cm^2, and the peak-to-valley ratio (ON:OFF ratio) was 1030:1 at 60 K.[59] Note that both the molecule and the contacts to each end of the molecule are asymmetric.

Reed and co-workers very carefully studied the *I(V,T)* characteristics of alkanethiol SAMs in the nanopore.[18] The *I(V,T)* measurements are necessary to rule out filimentary metal-based conduction. As discussed above, the nanopore devices were fabricated by deposition of a SAM of alkanethiol on a Au surface in the nanopore followed by very slow deposition of the top Au electrode at liquid nitrogen temperatures to ensure that thermal damage was not done to the SAM. Direct tunneling was proven to be the transport mechanism through the SAMs based on these measurements. The tunneling currents were fitted to theoretical calculations with a modified rectangular barrier model of direct tunneling. The barrier height Φ_B was found to be 1.42 ± 0.04 eV. By measuring the conductance of SAMs from alkanethiols of different chain lengths, the tunneling current displayed an exponential dependence on the molecular length that was found to be bias-dependent. This agreed with the existing theory of direct tunneling. A zero-field decay coefficient β_0 of 0.79 ± 0.01 Å^{-1} was measured.

X. Other Testbeds

Amlani and co-workers[60,61] developed a unique approach to a molecular electronics testbed by forming SAMs on Au electrodes separated by a 40−100 nm gap; Au nanoparticles were then trapped in the gap by applying an ac bias of 0.5−2.5 V at 1−10 MHz for 5−20 s. An illustration of the testbed is shown in Figure 25.

Scanning electron microscopy (SEM) verified that the nanoparticles were being trapped between the electrodes. Testing of the *I(V)* characteristics of the metal−molecule−metal−molecule−metal junction formed by **31**, Figure 26, showed NDR with two peaks, as could be expected of two SAMs formed in series. The authors state that the most probable circuit equivalent is two resonant tunneling diodes, an arrangement that is known to yield two NDR peaks.[62] Measurements were done in air; degradation was evident after a few sweeps. In different samples the *I(V)* profile changed due to variations in the number of nanoparticles trapped; clumps of nanoparticles could be trapped depending on the size of the gap and the size of the nanoparticles. No *I(V,T)*[18] studies were done. Testing of alkanethiols and unsubstituted OPEs in the testbed under similar conditions produced no NDR behavior.

With our collaborator Bard we measured charge transport through SAMs using tuning-fork-based scanning probe microscopy (SPM);[63] the apparatus is shown in Figure 27. The tuning fork allows for better detection and control of the approach of the SPM tip to the surface of the SAM.[64] Hexadecanethiol, OPE **1a**, and OPEs **32**−**39** and OP **40**, Figure 28, were tested.

The *I(V)* curves obtained using the tuning-fork-based SPM testbed for hexadecanethiol at low bias were symmetric around 0 V. The current increased exponentially with *V* at high bias voltage. In contrast, reversible peak-shaped *I(V)* characteristics, or NDR, were obtained for most of the nitro-substituted OPE SAMs, indicating that part of the conduction mechanism of the junctions involved resonance tunneling. For all of the SAMs the current decreased as the distance from the SPM tip to the surface of the SAM increased. For hexadecanethiol, β was nearly independent of tip bias and ranged from 1.3 to 1.4 Å^{-1}. For the nitro-based molecules, β was low and depended strongly on the tip bias, with values ranging from 0.15 Å^{-1} for OPE **36** to 0.50 Å^{-1} for OP

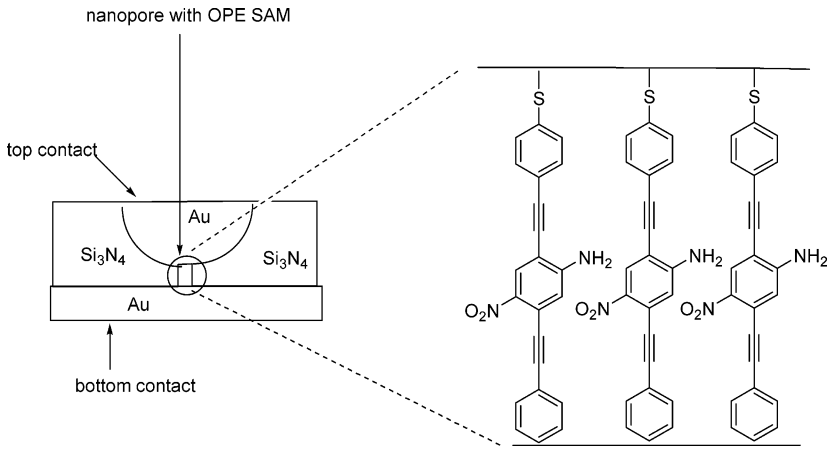

Figure 24. Nanopore testbed structure with an enlargement of the nanopore showing a small portion of the OPE SAM. Note that the thiolate−Au bond forms to the top contact due to the sequence of the process.

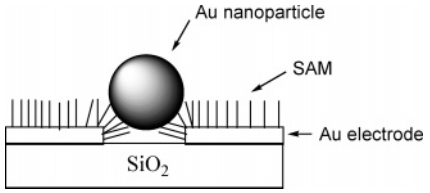

Figure 25. Testbed developed by Amlani and co-workers in which a Au nanoparticle is trapped between two electrodes covered by SAMs.

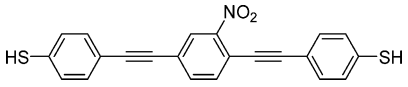

Figure 26. Molecule **31** tested by Amlani and co-workers in the metal−molecule−metal−molecule−metal junction.

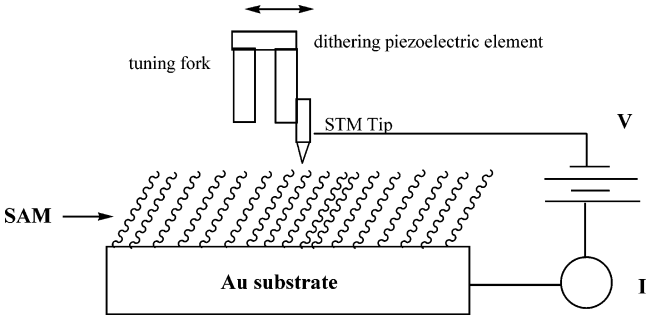

Figure 27. Representation of the measurement and formation of a metal−molecule−metal junction with a tuning-fork-based SPM tip containing a SAM on Au.

40 at a tip bias of −3.0 V. Charge storage was observed in the nitro-based molecules, as ∼25% of the charge collected in the negative scan was stored in the molecules and could be collected at positive voltages. A possible mechanism involving lateral electron hopping was proposed to explain the phenomenon. *I(V,T)*[18] measurements were not carried out to confirm the conduction mechanism.

In cross-bar-based testbeds made from Langmuir−Blodgett monolayers sandwiched between planar Pt and Ti metal electrodes,[65] "a generic switching mechanism dominated by electrode properties or electrode/molecule interfaces, rather than molecule-specific behavior" was observed. The authors concluded that the characteristics of the electrical measurements made on molecular electronic devices are due to a combination of the physical properties of the specific molecules *and* the physical properties of the metal electrodes *and* the physical properties of the interactions between the two.

Whitesides measured the electrical breakdown voltage (BDV, the maximum voltage sustained by the junction) of thiol-containing molecules in Hg−SAM/SAM−M′ assemblies[66] in which a drop of liquid Hg supporting a SAM was placed in contact with a SAM on a flat metal surface. The value of the BDV depended on the second metal in the order Ag > Hg > Cu > Au for SAMs formed from hexadecanethiol. The BDV increased as the packing density of the SAM increased and the tilt angle decreased. The BDV correlated well with the thickness of the packed hydrocarbon portion of the SAM; the thicker the layer, the higher the BDV.

Using the Ag−SAM/SAM−Hg system, Whitesides measured the rates of electron transport through the SAMs[67] and determined β values for alkanethiols (0.87 ± 0.1 Å^{-1}), OP thiols (0.61 ± 0.1 Å^{-1}), and benzylic derivatives of OP thiols (0.67 ± 0.1 Å^{-1}), all at an applied potential of 0.5 V, although the values of β did not vary significantly when the applied voltage was varied between 0.1 and 1 V. These results were similar to those obtained by Frisbie[30] and Bard[63] in that OP thiols were better conductors that alkanethiols.

Whitesides used the mercury drop testbed to develop a junction that rectified current.[68] In this embodiment a SAM formed on Ag or Au from a dialkyl disulfide containing a covalently linked tetracyanoquinodimethane group (Figure 29) was contacted with an alkanethiolate SAM on the Hg drop. At a potential of 1 V, the forward bias conductivitiy (Hg cathodic) was 7−11 times greater than the reverse bias conductivity (Hg anodic). The difference between the forward bias conductivity and the reverse bias conductivity increased with decreasing chain length of the alkanethiol in the Hg SAM.

By electrochemically depositing Au into the 70 nm diameter pores of polycarbonate track etch membranes, followed by alkanethiolate SAM formation and capping with electrolessly grown Au, Mallouk formed nanowires containing monolayer molecular junctions.[69] Nanowires assembled in a similar fashion but using the nitro OPE **1b** in the SAM were aligned between lithographically defined electrodes on a substrate and covered by a contact electrode to form devices that demonstrated room-temperature NDR with ON−OFF peak-to-valley

confirm the conduction mechanism.

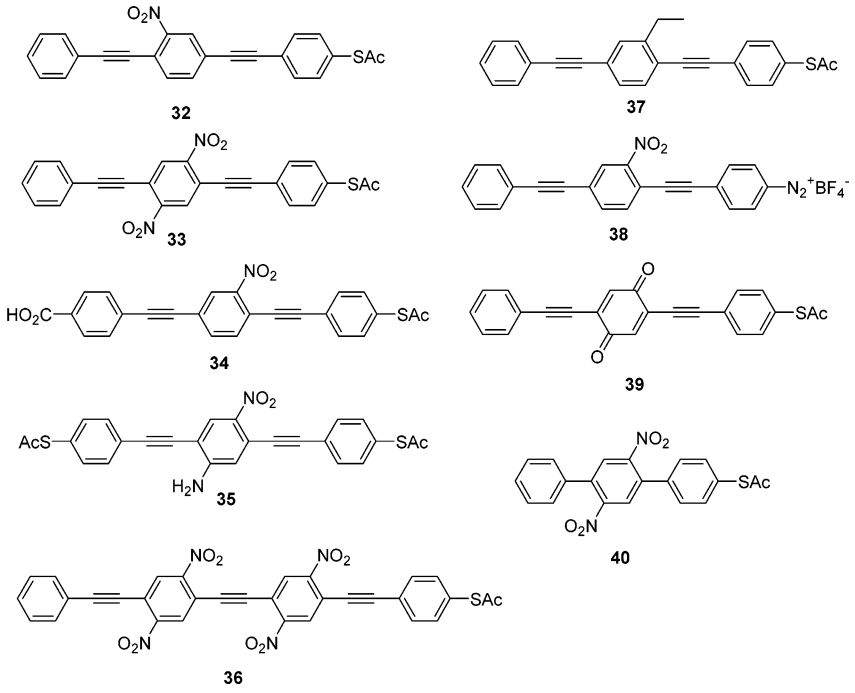

Figure 28. OPEs **32**−**39** and OP **40** tested in the tuning-fork-based SPM testbed.

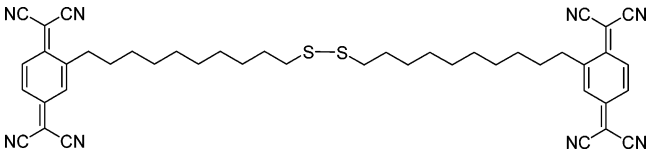

Figure 29. Tetracyanoquinodimethane-containing dialkyl disulfide that was used to form a SAM in Whitesides mercury drop assembly that demonstrated electrical rectification.

ratios of 1.80−2.21.[70] In a further application of this testbed, junction-containing nanowires were made using OPE **4**, alkanedithiol **25**, or OPV **26**.[71] In this case the bottom contacts were Au or Pd and the top caps were Ag or Pd. Room-temperature *I*(*V*) measurements indicated that junctions formed from the conjugated molecules **4** and **26** had conductances that were several orders of magnitude higher than the conductance of the junction formed from **25**, with the OPV **26** demonstrating the highest conductance. The symmetric Pd−molecule−Pd junctions yielded the best metal−molecule coupling and the highest conductance.

XI. Damage to SAMs by Deposition of Top Metal Electrodes

Grazing-incidence Fourier transform infrared (GI−FTIR) spectroscopy of SAMs after deposition of a top metal electrode[72] has been used to show that vapor deposition of Au or Al on OP dithiol SAMs reacts at the SAM/vacuum interface with the top thiol group, preventing metal penetration of the SAM, while OP monothiols do not have such protection and Au or Al can penetrate the SAM. The GI−FTIR evidence indicates that vapor deposition of Ti onto OP mono- and dithiol SAMs as well as the SAM from hexadecanethiol destroys the SAMs under the conditions used. Therefore, it is important, if possible, to analyze the organic SAM after deposition in testbeds where metal is deposited from the vapor phase to form a top contact.

XII. Summary and Conclusion

In summarizing the bulk of the cited literature, it is clear that in measuring the electrical properties of molecular electronic candidates the characteristics of the entire metal−molecule−metal junction must be considered. The top metal contact formed by deposition from the vapor phase, such as used in fabricating nanopores, is different than the top metal contact formed by a crossed-wire junction, STM tip, or cAFM tip. It is difficult if not impossible to disconnect the physical properties of the molecule from that of the metals to which it is attached.

The search for an easily constructed and useful testbed for measuring the electrical characteristics of metal−molecule−metal junctions in molecular electronics-based devices has included the development of methods based on crossed-wire junctions, mechanically controllable break junctions, cAFM, STM, molecular electronics on silicon surfaces, the NanoCell, nanopores, and several other devices. While all of these methods have provided important preliminary information that has fired the imagination of countless chemists around the world in designing new molecular electronics candidates, the testing results have not provided rigorous proof of the mechanism of action of molecular electronics candidates in their most realistic device embodiments.

On the basis of our review of the literature, the *I(V,T)* work done in the nanopore under very stringent controlled conditions has provided the best information, from a device physics point-of-view, as far as the mechanism of conduction within the molecular electronic SAMs. It is clear we have not reached the goal of an easily constructed and easily usable testbed as the nanopore is neither of those. The best approach may be

to use easier techniques such as cAFM and STM to compare the preliminary electrical characteristics of the various candidates and to follow up with the more rigorous nanopore testing to nail down the mode of conduction. Since for the first time in history we are operating at the nanoscale in determining the electrical properties of a few or individual molecules, it is not surprising that the method used to gather the most conclusive data is difficult to attain at best. At least it is not impossible. Therein lies the hope for future development.

Acknowledgment. The Defense Advanced Research Projects Agency, the Office of Naval Research, the Air Force Office of Scientific Research, the Army Research Office, The Department of Commerce National Institute of Standards and Technology, and the National Science Foundation supported this work. We thank Prof. Jorge Seminario of Texas A&M University for providing the cover art section associated with this review (row 3, third image from left).

References

(1) Tour, J. M. *Acc. Chem. Res.* **2000**, *33*, 791−804.
(2) Tour, J. M.; James, D. K. *Handbook of Nanoscience, Engineering and Technology*; Goddard, W. A., III, Brenner, D. W., Lyshevski, S. E., Iafrate, G. J., Eds.; CRC Press: New York, 2003; pp 4.1−4.28.
(3) Tour, J. M. *Molecular Electronics: Commercial Insights, Chemistry, Devices, Architecture and Programming*; World Scientific: River Edge, NJ, 2003.
(4) Hwang, J.-J.; Tour, J. M. *Tetrahedron* **2002**, *58*, 10387−10405.
(5) Dirk, S. M.; Tour, J. M. *Tetrahedron* **2003**, *59*, 287−293.
(6) Price, D. W., Jr.; Tour, J. M. *Tetrahedron* **2003**, *59*, 3131−3156.
(7) Flatt, A. K.; Dirk, S. M.; Henderson, J. C.; Shen, D. E.; Su, J.; Reed, M. A.; Tour, J. M. *Tetrahedron* **2003**, *59*, 8555−8570.
(8) Flatt, A. K.; Tour, J. M. *Tetrahedron Lett.* **2003**, *44*, 6699−6702.
(9) Stewart, M. P.; Maya, F.; Kosynkin, D. V.; Dirk, S. M.; Stapleton, J. J.; McGuiness, C. L.; Allara, D. L.; Tour, J. M. *J. Am. Chem Soc.* **2004**, *126*, 370−378.
(10) Ciszek, J. W.; Tour, J. M. *Tetrahedron Lett.* **2004**, *45*, 2801−2803.
(11) Metzger, R. M. *Chem. Rev.* **2003**, *103*, 3803−3834.
(12) Carroll, R. L.; Gorman, C. B. *Angew. Chem., Int. Ed.* **2002**, *41*, 4378−4400.
(13) Mantooth, B. A.; Weiss, P. S. *Proc. IEEE* **2003**, *91*, 1785−1802.
(14) Salomen, A.; Cahen, D.; Lindsay, S.; Tomfohr, J.; Engelkes, V. B.; Frisbie, C. D. *Adv. Mater.* **2003**, *15*, 1881−1890.
(15) Stapleton, J. J.; Harder, P.; Daniel, T. A.; Reinard, M. D.; Yao, Y.; Price, D. W.; Tour, J. M.; Allara, D. L. *Langmuir* **2003**, *19*, 8245−8255.
(16) Cai, L.; Yao, Y.; Yang, J.; Price, D. W., Jr.; Tour, J. M. *Chem. Mater.* **2002**, *14*, 2905−2909.
(17) Kushmerick, J. G.; Naciri, J.; Yang, J. C.; Shashidhar, R. *Nano Lett.* **2003**, *3*, 897−900.
(18) Lee, T.; Wang. W.; Reed, M. A. *Ann. N.Y. Acad. Sci.* **2003**, *1006*, 21−35.
(19) Weiss, P. S. *Science* **2004**, *303*, 1136−1137.
(20) Kushmerick, J. G.; Holt, D. B.; Yang, J. C.; Naciri, J.; Moore, M. H.; Shashidar, R. *Phys. Rev. Lett.* **2002**, *89*, 086802-1−086802-4.
(21) Pollack, S. K.; Naciri, J.; Mastrangelo, J.; Patterson, C. H.; Torres, J.; Moore, M.; Shashidar, R.; Kushmerick, J. G. *Langmuir* **2004**, *20*, 1838−1842.
(22) Biebuyck, H. A.; Whitesides, G. M. *Langmuir* **1993**, *9*, 1766−1770.
(23) Price, D. W., Jr.; Dirk, S. M.; May, F.; Tour, J. M. *Tetrahedron* **2003**, *59*, 2497−2518.
(24) Reed, M. A.; Zhou, C.; Muller, C. J.; Burgin, T. P.; Tour, J. M. *Science* **1997**, *278*, 252−254.
(25) Reichert, J.; Ochs, R.; Beckman, D.; Weber, H. B.; Mayor, M.; Löhneysen, H. v. *Phys. Rev. Lett.* **2002**, *88*, 176804-1−176804-4.
(26) Reichert, J.; Weber, H. B.; Mayor, M.; Löhneysen, H. v. *Appl. Phys. Lett*. **2003**, *82*, 4137−4139.
(27) Weber, H. B.; Reichert, J.; Weigend, F.; Ochs, R.; Beckmann, D.; Mayor, M.; Ahlrichs, R.; Löhneysen, H. v. *Chem. Phys.* **2002**, *281*, 113−125.
(28) Wold, D. J.; Frisbie, C. D. *J. Am. Chem. Soc.* **2000**, *122*, 2970−2971.
(29) Wold, D. J.; Frisbie, C. D. *J. Am. Chem. Soc.* **2001**, *123*, 5549−5556.
(30) Wold, D. J.; Haag, R.; Rampi, M. A.; Frisbie, C. D. *J. Phys. Chem. B* **2002**, *106*, 2813−2816.
(31) Rawlett, A. M.; Hopson, T. J.; Nagahara, L. A.; Tsui, R. K.; Ramachandran, G. K.; Lindsay, S. M. *Appl. Phys. Lett*. **2002**, *81*, 3043−3045.
(32) Cui, X. D.; Zarate, X.; Tomforh, J.; Sankey, O. F.; Primak, A.; Moore, A. L.; Moore, T. A.; Gust, D.; Harris, G.; Lindsay, S. M. *Nanotechnology* **2002**, *13*, 5−14.
(33) Slowinski, K.; Chamberlain, R. V.; Miller, C. J.; Majda, M. *J. Am. Chem. Soc.* **1997**, *119*, 910−911.
(34) Xu, B.; Xiao, X.; Tao, N. J. *J. Am. Chem. Soc.* **2003**, *125*, 16164−16165.
(35) Samori, P.; Rabe, J. P. *J. Phys. Condens. Matter* **2002**, *14*, 9955−9973.
(36) Chen, J.; Reed, M. A.; Asplund, C. L.; Cassell, A. M.; Myrick, M. L.; Rawlett, A. M.; Tour, J. M.; Van Patten, P. G. *Appl. Phys. Lett*. **1999**, *75*, 624−626.
(37) Dunbar, T. D.; Cygan, M. T.; Bumm, L. A.; McCarty, G. S.; Burgin, T. P.; Reinerth, W. A.; Jone, L., II; Jackiw, J. J.; Tour, J. M.; Weiss, P. S.; Allara, D. L. *J. Phys. Chem.* **2000**, *104*, 4880−4893.
(38) Donhauser, Z. J.; Price, D. W., II; Tour, J. M.; Weiss, P. S. *J. Am. Chem. Soc.* **2003**, *125*, 11462−11463.
(39) Donhauser, Z. J.; Mantooth, B. A.; Kelly, K. F.; Bumm, L. A.; Monnell, J. D.; Stapleton, J. J.; Price, D. W., Jr.; Rawlett, A. M.; Allara, D. L.; Tour, J. M.; Weiss, P. S. *Science* **2001**, *292*, 2303−2307.
(40) Ishida, T. I.; Mizutani, W.; Choi, N.; Akiba, U.; Fujihira, M.; Tokumoto, H. *J. Phys. Chem. B* **2000**, *104*, 11680−11688.
(41) Ishida, T.; Mizutani, W.; Akiba, U.; Umemura, K.; Inoue, A.; Choi, N.; Fujihara, M.; Tokumoto, H. *J. Phys. Chem. B* **1999**, *193*, 1686−1690.
(42) Yang, G.; Qian, Y.; Engtrakul, C.; Sita, L. R.; Liu, G. *J. Phys. Chem. B* **2000**, *104*, 9059−9062.
(43) Gorman, C. B.; Carroll, R. L.; Fuierer, R. R. *Langmuir* **2001**, *17*, 6923−6930.
(44) Patrone, L.; Palacin, S.; Bourgoin, J. P.; Lagoute, J.; Zambelli, T.; Gauthier, S. *Chem. Phys.* **2002**, *281*, 325−332.
(45) Seminario, J. M.; Zacarias, A. G.; Tour, J. M. *J. Am.Chem. Soc*. **1999**, *121*, 411−416.
(46) Yasuda, S.; Nakamura, T.; Matsumoto, M.; Shigekawa, H. *J. Am. Chem. Soc.* **2003**, *125*, 16430−16433.
(47) Wassel, R. A.; Fuierer, R. R.; Kim, H.; Gorman, C. B. *Nano Lett.* **2003**, *3*, 1617−1620.
(48) Wassel, R. A.; Credo, G. M.; Fuierer, R. R.; Feldheim, D. L.; Gorman, C. B. *J. Am. Chem. Soc.* **2004**, *126*, 295−300.
(49) Blum, A. S.; Yang, J. C.; Shashidar, R.; Ratna, B. *Appl. Phys. Lett.* **2003**, *82*, 3322−3324.
(50) Kosynkin, D. V.; Tour, J. M. *Org. Lett.* **2001**, *3*, 993.
(51) Stewart, M. P.; Maya, F.; Kosynkin, D. V.; Dirk, S. M.; Stapleton, J. J.; McGuiness, C. L.; Allara, D. L.; Tour, J. M. *J. Am. Chem Soc.* **2004**, *126*, 370−378.
(52) Wang, W.; Lee, T.; Kamdar, M.; Reed, M. A.; Stewart, M. P.; Huang, J. J.; Tour, J. M. *Ann. N.Y. Acad. Sci.* **2003**, *1006*, 36−47.
(53) Wang, W.; Lee, T.; Reed, M. A.; Stewart, M. P.; Huang, J. J.; Tour, J. M. *Superlattices Microstruct.* **2003**, *33*, 213.
(54) Guisinger, N. P.; Greene, M. E.; Basu, R.; Baluch, A. S.; Hersam, M. C. *Nano Lett.* **2004**, *4*, 55−59.
(55) Tour, J. M.; Cheng, L.; Nackashi, D. P.; Yao, Y.; Flatt, A. K.; St. Angelo, S. K.; Mallouk, T. E.; Franzon, P. D. *J. Am. Chem. Soc.* **2003**, *125*, 13279−13283.
(56) Tour, J. M.; Van Zandt, W. L.; Husband, C. P.; Husband, S. M.; Wilson, L. S.; Franzon, P. D.; Nackashi, D. P. *IEEE Trans. Nanotechnol.* **2002**, *1*, 100.
(57) Chen J.; Wang, W.; Reed, M. A.; Rawlett, A. M.; Price, D. W.; Tour, J. M. *Mater. Res. Soc. Proc.* **2001**, *582*, H3.2.1−H3.2.5.
(58) Reed, M. A.; Chen, J.; Rawlett, A. M.; Price, D. W.; Tour, J. M. *Appl. Phys. Lett.* **2001**, *78*, 3735−3737.
(59) Chen, J.; Reed, M. A.; *Chem. Phys.* **2002**, *281*, 127−145.
(60) Amlani, I.; Rawlett, A. M.; Nagahara, L. A.; Tsui, R. K. *Appl. Phys. Lett.* **2002**, *80*, 2761−2763.
(61) Amlani, I.; Rawlett, A. M.; Nagahara, L. A.; Tsui, R. *J. Vac. Sci. Technol. B* **2002**, *20*, 2802−2805.
(62) Shen, J.; Kramer, G.; Tehrani, S.; Goronkin, H.; Tsui, R. *IEEE Electron Device Lett.* **1995**, *16*, 178.
(63) Fan, F.-R. F.; Yang, J.; Cai, L.; Price, D. W., Jr.; Dirk, S. M.; Kosynkin, D. V.; Yao, Y.; Rawlett, A. M.; Tour, J. M.; Bard, A. J. *J. Am. Chem. Soc.* **2002**, *124*, 5550−5560.
(64) Karrai, K.; Grober, R. D. *Appl. Phys. Lett.* **1995**, *66*, 1842−1844.
(65) Stewart, D. R.; Ohlberg, D. A. A.; Beck, P. A.; Chen, Y.; Williams, R. S.; Jeppesen, J. O.; Nielsen, K. A.; Stoddart, J. F. *Nano Lett.* **2004**, *4*, 133−136.
(66) Haag, R.; Rampi, M. A.; Holmlin, R. E.; Whitesides, G. M. *J. Am. Chem. Soc.* **1999**, *121*, 7895−7906.

(67) Holmlin, R. E.; Haag, R.; Chabinye, M. L.; Ismagilov, R. F.; Cohen, A. E.; Terfort, A.; Rampi, M. A.; Whitesides, G. M. *J. Am. Chem. Soc.* **2001**, *123*, 5075−5085.
(68) Chabinyc, M. L.; Chen, X.; Holmlin, R. E.; Jacobs, H.; Skulason, H.; Frisbie, C. D.; Mujica, V.; Ratner, M. A.; Rampi, M. A.; Whitesides, G. M. *J. Am. Chem. Soc.* **2002**, *124*, 11730−11736.
(69) Mbindyo, J. K. N.; Mallouk, T. E.; Mattzela, J. B.; Kratochvilova, I.; Razavi, R.; Jackson, T. N.; Mayer, T. S. *J. Am. Chem. Soc.* **2002**, *124*, 4020−4026.
(70) Kratochvilova, I.; Kocirik, M.; Zambova, A.; Mbindyo, J.; Mallouk, T. E.; Mayer, T. S. *J. Mater. Chem.* **2002**, *12*, 2927−2930.
(71) Cai, L. T.; Skulason, H.; Kushmerick, J. G.; Pollack, S. K.; Naciri, J.; Shashidhar, R.; Allara, D. L.; Mallouk, T. E.; Mayer, T. S. *J. Phys. Chem. B* **2004**, *108*, 2827−2832.
(72) De Boer, B.; Frank, M. M.; Chabal, Y. J.; Jianh, W.; Garfunkel, E.; Bao, Z. *Langmuir* **2004**, *20*, 1539−1542.

CM049648R